Organic & Biomolecular Chemistry

ROYAL SOCIETY OF CHEMISTRY

COMMUNICATION

View Article Online
View Journal | View Issue

Check for updates

Cite this: *Org. Biomol. Chem.*, 2025, **23**, 5313

Received 16th April 2025,
Accepted 7th May 2025

DOI: 10.1039/d5ob00629e

rsc.li/obc

Microenvironmental engineering of active sites for selective catalytic hydrolysis of acetals†

Mansi Sharma and Yan Zhao *

Rational design of synthetic catalysts that mimic enzymes in catalysis and substrate selectivity is a long-standing goal of chemists. We report bottom-up synthesis of artificial acetal hydrolase that hydrolyzes its substrate with high selectivity under otherwise impossible neutral and basic conditions. Our synthetic method allows facile modification of the active site, including introduction of a local water pool near the acetal group of the bound substrate to alter the catalytic mechanism or installment of a secondary catalytic group to enhance the catalytic activity.

Other than their stability, enzymes are chemists' dream catalysts probably in every aspect of performance—*e.g.*, catalytic efficiency under mild conditions even for some of the most challenging reactions such as C–H functionalization, substrate-, regio- and stereo-selectivity, and response to environmental stimuli, to name a few. Enzymes may be modified by site-directed mutagenesis at specific locations but this tool is best suited for enzyme mechanism dissection instead of performance enhancement.[1] A powerful way to improve enzymes is directed evolution, *via* iterations of random mutations of the enzymatic gene, protein expression, and screening and selection of the expressed proteins for desired traits.[2]

A long-standing goal of chemists is to build synthetic mimics of enzymes (*i.e.*, artificial enzymes).[3–6] If made to have enzyme-rivaling activities and selectivity, due to their higher stability such catalysts may enable catalytic reactions incompatible with fragile biomolecules. Without the molecular production machinery in biology, however, it is much more difficult for chemists to construct and improve such catalysts. Not only would they have to build a custom-tailored pocket for substrate binding, but the pocket also would need to have catalytic groups positioned precisely for the catalytic transformation. If further fine-tuning of the active site is required—*e.g.*, introduction of auxiliary catalytic groups or tuning the polarity of the active site—the synthetic challenge becomes unimaginable.

Instead of building a pocket-forming molecular scaffold by direct chemical synthesis, molecular imprinting builds a polymer network around molecular "molds" or template molecules.[7–9] After removal of the templates, imprinted pockets are left behind conveniently within the polymer. With these tailor-made pockets, molecularly imprinted polymers have broad applications in chemistry and biology,[10–12] including in enzyme-mimicking catalysis.[13–20]

In this work, we demonstrate facile construction of tunable active sites inside water-soluble imprinted nanoparticles. The synthetic strategy allows the active site of our artificial enzyme to be fine-tuned for selective hydrolysis of acetals.[21–24] Acetals are prevalent functional groups in natural products, notably as the glycosidic linkages between the monosaccharide building blocks in carbohydrate oligomers and polymers. The microenvironmental engineering of the active site is shown to modulate not only the catalytic activity but also the mechanism of hydrolysis.

The model substrate for our artificial acetal hydrolase is aryloxy acetal **S1**, whose simple structure and convenient monitoring of its hydrolysis by UV-vis spectroscopy make it well-suited for testing design hypotheses. To build an active site for **S1**, we synthesized thiourea **T1** as the template and used commercially available 4-vinylbenzoic acid (4VB) as the functional monomer (FM). Thiourea and carboxylic acid are known to interact strongly through two hydrogen bonds even in polar solvents.[25] Our expectation is that **T1** and 4VB will form a hydrogen-bonded template–FM complex within the micelles of surfactant **1** (Scheme 1a), facilitated by the nonpolar microenvironment of micelles.[26,27]

The template-containing micelles are first cross-linked on the surface by diazide **2** *via* a copper-catalyzed alkyne–azide click reaction (Scheme 1a, step a), with some alkynes intentionally left for another round of click reaction with monoa-

Department of Chemistry, Iowa State University, Ames, Iowa 50011-3111, USA. E-mail: zhaoy@iastate.edu; Tel: +1-515-294-5845

†Electronic supplementary information (ESI) available: Synthetic procedures, characterization data, ITC titration curves, additional data, and NMR spectra. See DOI: https://doi.org/10.1039/d5ob00629e

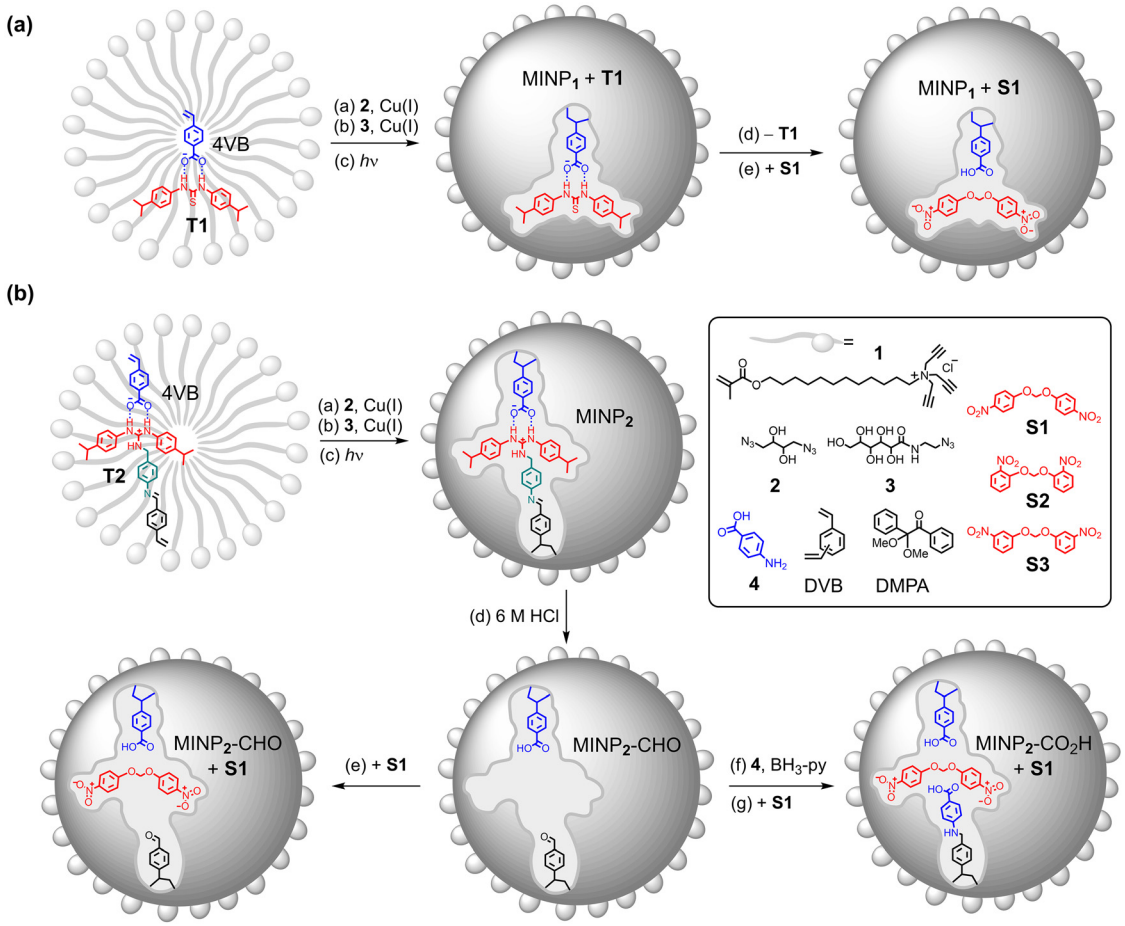

Scheme 1 Preparation of molecularly imprinted nanoparticles (MINPs) for catalytic hydrolysis of acetals (**S1**–**S3**).

zide **3** (step b). (Surface functionalization installs a layer of hydrophilic ligands on the micelle surface, which enhance the hydrophilicity of the final molecularly imprinted nanoparticles (MINPs) and facilitate their purification by simple precipitation and solvent washing.) Molecular imprinting largely occurs during the core polymerization in step c, among the methacrylates on the surfactant tails, the divinylbenzene (DVB) molecules solubilized in the micelles, and the vinyl group of 4VB, induced by the photolysis of 2,2-dimethoxy-2-phenylaceto-phenone (DMPA, a photoinitiator).

The preparation of the MINPs and their characterization are reported in the ESI.† ^{1}H NMR spectroscopy allows us to monitor the cross-linking of the micelles (Fig. S1†). Dynamic light scattering (DLS) affords the size distribution of the nanoparticles (Fig. S2–S4†). The particle size was confirmed by transmission electron microscopy (TEM, Fig. S5†).

As shown in Scheme 1a, $MINP_1$, *i.e.*, the MINP prepared with **T1** as the template, has 4VB polymerized into the micelle core. The polymerized FM turns into a binding group for the template during molecular imprinting. Upon removal of the noncovalently bound template, an active site is created that has the correct size and shape for substrate **S1** and a carboxylic acid in close proximity to the acetal oxygens for catalytic hydrolysis.

Consistent with our design, $MINP_1$ strongly catalyzes the hydrolysis of **S1** in aqueous buffer, even under strongly basic conditions (Fig. 1). In contrast, hydrolysis of the acetal is negligible under basic conditions and is slow at pH 6 in the presence of nonimprinted nanoparticles (NINPs) prepared without the template.

These preliminary results are promising. A substrate-resembling thiourea template in our design allows a substrate-tai-

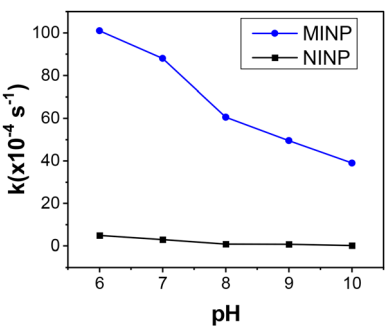

Fig. 1 Dependence of acetal hydrolysis of **S1** catalyzed by $MINP_1$ *versus* NINP at 40 °C. [**S1**] = 100 μM. [$MINP_1$] = [NINP] = 5.0 μM.

lored active site to be produced in a one-pot reaction within 2 days for acetal hydrolysis, without any complicated synthesis or postmodification. Catalytic hydrolysis under basic conditions[22,28] is only possible if a locally acidic group is present. Carboxylic acids typically have a pK_a of 4–5 in aqueous solution. But a hydrophobic microenvironment is known to shift the pK_a to higher values in enzyme active sites.[29] Meanwhile, neighboring positive charges can help the deprotonation of an acid and shift its pK_a to a lower value.[30] Both factors are present in our cross-linked cationic micelles, but the local hydrophobicity seems to dominate in our catalyst, making it possible to hydrolyze acetals under basic conditions.

Having confirmed the design hypothesis, we set our next goal as the fine-tuning of the active site for higher activity. Template **T2** has a guanidinium group to bind the 4VB FM (Scheme 1b). More importantly, this template has a cleavable imine bond and polymerizable vinyl. The resulting MINP$_2$ thus has both the template and the FM polymerized into the micelle core. The imine bond is then hydrolyzed under acidic conditions. The resulting MINP$_2$–CHO has the same carboxylic acid as the catalytic group as MINP$_1$, but it contains a vacant pocket near the acetal group of the bound substrate, after removal of the dark green substructure of the template during post-modification (Scheme 1b). Thus, a localized water pool is potentially created during the catalysis. Separately, reductive amination of MINP$_2$–CHO with 4-aminobenzoic acid (**4**) introduces a second carboxylic acid in the active site as an auxiliary catalytic group.

The reaction rate for the catalytic hydrolysis of **S1** follows the order of MINP$_1$ < MINP$_2$–CHO < MINP$_2$–CO$_2$H (Fig. 2a). Hence, both the localized water pool and the auxiliary carboxylic acid are helpful to the catalysis. To understand the mechanism of hydrolysis in these MINPs, we measured the kinetic solvent effects (KIE) for these catalytic reactions. The most common mechanism of acetal hydrolysis is A1,[31–33] in which a fast protonation of an acetal oxygen is followed by the rate-limiting removal of an alcohol as the leaving group (4-nitrophenol in the case of **S1**). This mechanism is characterized by an inverse KIE of $k(H_2O)/k(D_2O)$ = 0.25–0.50. Another possible mechanism is A2, in which the removal of alcohol/phenol is assisted by the nucleophilic attack by a water molecule on the acetal carbon. Typically, the KIE for the A2 mechanism ranges from 0.55 to 0.80.[31–33] As shown in Table 1, the KIE values suggest that the hydrolysis of **S1** by both MINP$_1$ and MINP$_2$–CO$_2$H happens through the A1 mechanism but that by MINP$_2$–CHO takes the A2 pathway. In these experiments, the pD value was determined by adding 0.4 to the reading of a pH meter, to compensate for the different dissociation constants of water and D$_2$O.[34]

The change of mechanism in the catalytic hydrolysis is interesting. MINP$_2$–CHO is the only catalyst with an "empty" pocket near the bound substrate. The pocket is expected to be filled with water molecule(s) during the reaction, which could help the A2 mechanism by providing the nucleophile near the reactive center. In addition, the water molecules could increase the polarity of the active site, which could also be helpful to the stabilization of the charge-separated transition state. For both MINP$_1$ and MINP$_2$–CO$_2$H, **S1** is expected to fit snuggly in the active site. Lack of water molecules opposite to the departing phenol could be a reason why the A2 mechanism is not favored in these two cases.

MINP$_2$–CO$_2$H is the most active catalyst among the three. Its double acid motif mimics those in the active sites of glycosidase enzymes.[35,36] Cooperative actions between the two are known to help both natural enzymes[35,36] and small molecule enzyme models.[37,38] It is encouraging that catalytic motifs copied from nature also perform strongly in the biomimetic artificial enzymes. MINP$_2$–CO$_2$H, indeed, follows enzyme-like Michaelis–Menten kinetics, with a Michaelis constant (K_m) of 122 μM and a catalytic turnover (k_{cat}) of 1.03 min^{-1}, affording a catalytic efficiency of k_{cat}/K_m = 141 M^{-1} s^{-1} (Fig. 2b).

Enzymes can distinguish closely related compounds through their substrate-tailored active sites. MINP$_2$–CO$_2$H similarly is able to distinguish the substitution pattern on the phenyl rings of the substrate. As shown in Fig. 3, the *para* derivative is clearly favored by our artificial acetal hydrolase, whether tested individually (Fig. 3a) or together (Fig. 3b). This is expected from the *para* isopropyl groups on the template (**T2**). NINPs continue to show low activity in these experiments.

In summary, micellar imprinting gives a facile method to create functionalized pockets inside a water-soluble cross-linked polymeric nanoparticle. The nanoconfinement during micellar imprinting[39] is known to afford an extraordinary imprint/nonimprint ratio in binding, with numbers reaching hundreds[40] and even 10 000 sometimes.[41] MINPs can distinguish the addition,[39] removal,[39] and shift[42] of a single

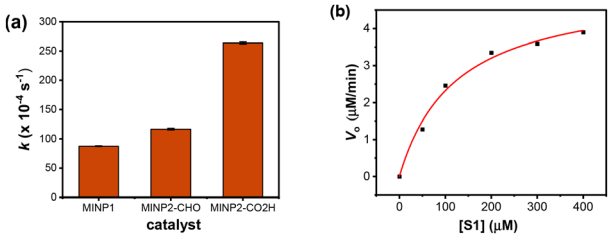

Fig. 2 (a) Comparison of the rate of hydrolysis of **S1** at pH 7 catalyzed by different MINPs at 40 °C in 10 mM HEPES buffer. [**S1**] = 100 μM. [MINP] = 5.0 μM. (b) Michaelis–Menten plot for the hydrolysis of substrate **S1** by MINP$_2$–CO$_2$H in a 10 mM HEPES buffer (pH 7.0) at 40 °C.

Table 1 Solvent kinetic isotope effects for the hydrolysis of **S1** catalyzed by MINPs[a]

Entry	Catalyst	k_{H_2O} (× 10^{-4} s^{-1})	k_{D_2O} (× 10^{-4} s^{-1})	k_{H_2O}/k_{D_2O}
1	MINP$_1$	87.5 ± 0.7	210.3 ± 4.0	0.42
2	MINP$_2$–CHO	116.7 ± 1.5	193.7 ± 5.7	0.60
3	MINP$_2$–CO$_2$H	264.0 ± 2	898 ± 2.7	0.29

[a] Reaction rates were measured at 40 °C in HEPES buffer at pH 7. [**S1**] = 100 μM. [MINPs] = 5 μM.

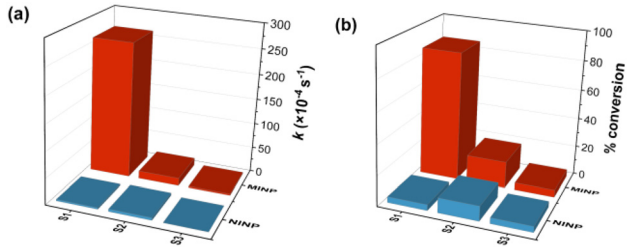

Fig. 3 (a) Substrate selectivity of $MINP_2$–CO_2H in the catalytic hydrolysis of **S1–3**. The reaction rate was monitored by UV at 40 °C in a 10 mM HEPES buffer at pH 7.0. (b) Selectivity of $MINP_2$–CO_2H in the catalytic hydrolysis of an equimolar mixture of **S1–3**. Reactions were performed in duplicate at 40 °C for 4 h in 10 mM HEPES buffer at pH 7.0. Dibromomethane was used as an internal standard. [**S1**] = [**S2**] = [**S3**] = 2.0 mM. [MINP] = 0.10 mM.

methyl (or methylene) group in the guest. Direct correlation between the size/shape of the thiourea template and the substrate selectivity of the MINP artificial acetal hydrolase in this work suggests that the platform is well-suited for rational design of active sites. Importantly, microenvironmental engineering of the active site, which is labor-intensive in enzymes and extremely challenging with small-molecule-based artificial enzymes, can be readily achieved with the imprinted micelles *via* different template molecules and suitable post-modification.

Data availability

The data supporting this article have been included as part of the ESI.†

Conflicts of interest

There are no conflicts to declare.

Acknowledgements

We thank the NSF (CHE-2246635) for financial support.

References

1 C. Wagner and S. Benkovic, *Trends Biotechnol.*, 1990, **8**, 263–270.
2 H. Renata, Z. J. Wang and F. H. Arnold, *Angew. Chem., Int. Ed.*, 2015, **54**, 3351–3367.
3 R. Breslow, *Artificial enzymes*, Wiley-VCH, Weinheim, 2005.
4 R. Breslow, *Acc. Chem. Res.*, 1995, **28**, 146–153.
5 A. J. Kirby and F. Hollfelder, *From enzyme models to model enzymes*, Royal Society of Chemistry, Cambridge, UK, 2009.
6 M. Raynal, P. Ballester, A. Vidal-Ferran and P. W. N. M. van Leeuwen, *Chem. Soc. Rev.*, 2014, **43**, 1734–1787.
7 G. Wulff, *Chem. Rev.*, 2002, **102**, 1–28.
8 K. Haupt and K. Mosbach, *Chem. Rev.*, 2000, **100**, 2495–2504.
9 L. Ye and K. Mosbach, *Chem. Mater.*, 2008, **20**, 859–868.
10 J. Pan, W. Chen, Y. Ma and G. Pan, *Chem. Soc. Rev.*, 2018, **47**, 5574–5587.
11 H. Zhang, *Adv. Mater.*, 2020, **32**, 1806328.
12 K. Haupt, P. X. Medina Rangel and B. T. S. Bui, *Chem. Rev.*, 2020, **120**, 9554–9582.
13 G. Wulff and J. Liu, *Acc. Chem. Res.*, 2012, **45**, 239–247.
14 S. Muratsugu, S. Shirai and M. Tada, *Tetrahedron Lett.*, 2020, **61**, 151603.
15 N. Kirsch, J. Hedin-Dahlström, H. Henschel, M. J. Whitcombe, S. Wikman and I. A. Nicholls, *J. Mol. Catal. B: Enzym.*, 2009, **58**, 110–117.
16 A. Servant, K. Haupt and M. Resmini, *Chem. – Eur. J.*, 2011, **17**, 11052–11059.
17 X. Shen, C. Huang, S. Shinde, K. K. Jagadeesan, S. Ekström, E. Fritz and B. Sellergren, *ACS Appl. Mater. Interfaces*, 2016, **8**, 30484–30491.
18 Y. Yuan, Y. Yang, M. Faheem, X. Zou, X. Ma, Z. Wang, Q. Meng, L. Wang, S. Zhao and G. Zhu, *Adv. Mater.*, 2018, **30**, 1800069.
19 S. Li, P. A. Lieberzeit, S. Piletsky and A. P. F. Turner, *Smart polymer catalysts and tunable catalysis*, Elsevier, Amsterdam, Netherlands; Cambridge, MA, 2019.
20 S. Striegler, B. Sharma and I. Orizu, *ACS Catal.*, 2020, **10**, 14451–14456.
21 D. T. Chou, J. Zhu, X. Huang and A. J. Bennet, *J. Chem. Soc., Perkin Trans. 2*, 2001, 83–89.
22 M. D. Pluth, R. G. Bergman and K. N. Raymond, *J. Org. Chem.*, 2009, **74**, 58–63.
23 Q. Zhang and K. Tiefenbacher, *J. Am. Chem. Soc.*, 2013, **135**, 16213–16219.
24 K. Li, K. Wu, Y.-Z. Fan, J. Guo, Y.-L. Lu, Y.-F. Wang, G. Maurin and C.-Y. Su, *Natl. Sci. Rev.*, 2022, **9**, nwab155.
25 V. Blažek Bregović, N. Basarić and K. Mlinarić-Majerski, *Coord. Chem. Rev.*, 2015, **295**, 80–124.
26 J. S. Nowick, J. S. Chen and G. Noronha, *J. Am. Chem. Soc.*, 1993, **115**, 7636–7644.
27 M. D. Arifuzzaman and Y. Zhao, *J. Org. Chem.*, 2016, **81**, 7518–7526.
28 M. D. Pluth, R. G. Bergman and K. N. Raymond, *Science*, 2007, **316**, 85–88.
29 D. Matulis and V. A. Bloomfield, *Biophys. Chem.*, 2001, **93**, 37–51.
30 J. D. Henao, Y.-W. Suh, J.-K. Lee, M. C. Kung and H. H. Kung, *J. Am. Chem. Soc.*, 2008, **130**, 16142–16143.
31 T. H. Fife, *Acc. Chem. Res.*, 1972, **5**, 264–272.
32 E. Cordes and H. Bull, *Chem. Rev.*, 1974, **74**, 581–603.
33 S. R. Wann and M. M. Kreevoy, *J. Org. Chem.*, 1981, **46**, 419–423.
34 R. A. Gibbs, P. A. Benkovic, K. D. Janda, R. A. Lerner and S. J. Benkovic, *J. Am. Chem. Soc.*, 1992, **114**, 3528–3534.
35 D. L. Zechel and S. G. Withers, *Acc. Chem. Res.*, 2000, **33**, 11–18.
36 D. L. Zechel and S. G. Withers, *Curr. Opin. Chem. Biol.*, 2001, **5**, 643–649.

37 E. Anderson and T. H. Fife, *J. Am. Chem. Soc.*, 1973, **95**, 6437–6441.
38 K. E. Dean and A. J. Kirby, *J. Chem. Soc., Perkin Trans. 2*, 2002, 428–432.
39 K. Chen and Y. Zhao, *Org. Biomol. Chem.*, 2019, **17**, 8611–8617.
40 L. Duan, M. Zangiabadi and Y. Zhao, *Chem. Commun.*, 2020, **56**, 10199–10202.
41 M. Zangiabadi and Y. Zhao, *ACS Appl. Polym. Mater.*, 2020, **2**, 3171–3180.
42 J. K. Awino, R. W. Gunasekara and Y. Zhao, *J. Am. Chem. Soc.*, 2017, **139**, 2188–2191.